Deterministic Self-Morphing of Soft-Stiff Hybridized Polymeric Films for Acoustic Metamaterials

Heng Deng,[||] Xianchen Xu,[||] Cheng Zhang, Jheng-Wun Su, Guoliang Huang,* and Jian Lin*

Read Online

ACCESS | 📊 Metrics & More | 📄 Article Recommendations | 🆂🅸 Supporting Information

ABSTRACT: We reported a soft-stiff hybridized polymeric film that can self-morph to dedicated three-dimensional (3D) structures for application in acoustic metamaterials. The hybridized film was fabricated by laterally adhering a soft and responsive poly(N-isopropylacrylamide) (PNIPAM) hydrogel to stiff and passive SU-8 patterns. Upon thermal stimulation, deformation of the tough PNIPAM hydrogel was locally constrained by the stiff SU-8 patterns, thereby causing laterally nonuniform strain to their interfaces for mechanically buckling the hybridized films to 3D structures. Combined with finite element analysis, we demonstrated that the stiff SU-8 patterns effectively alleviated the uncontrollability and uncertainty during the self-morphing process, which was caused by unexpected mutual deformation between the active and passive domains in the self-morphing materials. Therefore, deterministic self-buckling to dedicated 3D structures was physically realized such as a wave-shaped peak-valley structure, 3D checkerboard patterns, and Gaussian curved surfaces from the hybridized polymeric films. Finally, we demonstrated that the self-morphed 3D structures with predesigned patterns can be used as acoustic materials for subwavelength noise control. This transformative way of constructing 3D structures by self-morphing of the hybridized polymeric films will be a substantial progress in fabricating smart and multifunctional materials for widespread applications in metamaterials, soft robotics, and 3D electronics.

KEYWORDS: assembly, self-morphing, responsive, hydrogel, metamaterials
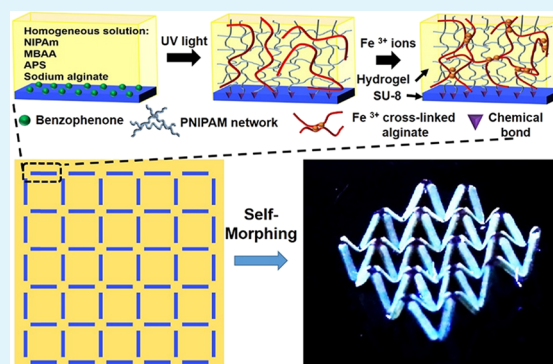
INTRODUCTION

Orderly arrangement of soft and stiff components in living organisms can be widely found in nature, which allows them to fully exploit synergistic benefits from both components. For instance, strong and tough biological materials such as shell and bone are hierarchical composites composed of stiff inorganics and soft biopolymers.[1] The skin of a chameleon contains periodically patterned stiff guanine crystals on a soft dermal layer. Once responding to environment, it exhibits shape transformation for scattering light with specific wavelengths, thus showing a function of disguising.[2,3] Researchers have been inspired by such strategies for designing and fabricating engineered materials with multifunctionalities. For instance, the soft and stiff materials have been periodically and hierarchically integrated to fabricate composites with optimized mechanical properties.[4,5] In mechanical metamaterials, the soft and hard materials were spatially and periodically patterned to create band structures and to break the time-reversal symmetry, laying novel paradigms of controlling the elastic and acoustic waves.[6−8] The remarkable characteristic of these three-dimensional (3D) structures is that their properties are quite sensitive to structural details of the soft and stiff materials. To fully explore the potentials of these hybrid structures, novel fabrication techniques that can realize delicate

structures consisting of multimode materials become urgent. Although several techniques such as additive manufacturing have been applied to directly fabricate these structures,[9,10] associated cost and time often exponentially increase with complexity of the shapes. In addition, a much narrower selection of materials can be effectively operated in three-dimensional (3D) printing techniques, thereby making printed structures have almost no access to materials (e.g., semiconductors and metals) and their resulting devices, which is a handicap to achieve multifunctionalities in the fabricated 3D structures.

A recently developed shape-morphing-induced assembly method, as demonstrated by us and others,[11−13] can transform two-dimensional (2D) planar sheets to complex 3D structures, thereby drawing tremendous attention. The most commonly used strategy for realizing 2D-to-3D shape-morphing is to utilize shape programmable materials,[14] which are often

stimuli-responsive polymers, hydrogels, and organogels.[12,15−21] These materials transform their shapes from planar sheets to 3D architectures upon external stimuli.[14,15,22−25] Compared to the direct 3D fabrication techniques, it possesses some superior advantages. First, fabrication of 2D responsive films can employ scalable planar fabrication processes. Second, a target 3D structure can be packed in a temporary and compact 2D state and then self-morphed to a final 3D state by stimuli in an on-demand manner. Third, it is applicable across material classes ranging from flexible polymers to brittle inorganics and can realize 3D structures in length scales ranging from tens of nanometers to centimeters.[26−29] Thus, this method has proved to be propitious in emerging fields such as energy harvesting, metamaterials, soft robotics, and sensors.[14,30−33] Despite significant progress made in this field, there still exists the problem of adopting such a shape-morphing method to realize deterministic 3D architectures with precise unit geometries.

This is because the general mechanism of 3D shape-morphing arises from cooperative interactions of active and passive components in the hybridized materials upon external stimulation, thus usually leading to uncontrollable and unpredictable deformation.[15,23,24] Such mutual deformation greatly increases complexity of the nonlinear mechanics in the self-morphing process, causing significant negative consequence to the self-morphed 3D structures. First, it may cause mechanical instability, which leads to the formed 3D structures with multiple self-buckling modes.[23,34] Second, it makes geometries of units easier to be affected by deformation of the neighboring ones, increasing the self-morphing uncertainty. Finally, it always leads to rough edges or facets in the 3D structures.[23] Thus, the resulting 3D structures barely reach the precision level, which limits their applications for developing new functional materials.

To overcome these technical barriers, we reported 3D structures made from deterministic self-morphing of responsive polymeric films, hybridized ones, that are fabricated by laterally adhering active poly(*N*-isopropylacrylamide (PNIPAM) hydrogel to passive SU-8 patterns, for applications in the acoustic metamaterials. From experimental studies, we found that the passive SU-8 patterns were stiff enough to resist the interfacial stress that results from shrinkage of the active PNIPAM hydrogel, making the shape deformation be confined in the active domains. Numerical studies disclosed that the stiff SU-8 patterns increased energy barrier, which is the energy needed to be overcome for the shape to be transformed from an original planar shape to a buckled 3D one, thereby effectively alleviating uncontrollability and uncertainty of self-morphing behaviors. In addition, the resulting 3D structures showed sharp edges and facets. With these advantages, a serial of delicate 3D structures were fabricated, including a wave-shaped peak-valley structure, 3D checkerboard patterns, and Gaussian surfaces that are usually not attainable in pure hydrogel systems. Finally, we demonstrated that some self-morphed 3D buckling structures predesigned by numerical simulation showed sonic band gaps, paving a new route to the application in acoustic metamaterials.

■ RESULTS AND DISCUSSION

The soft-stiff hybridized polymeric films were fabricated by laterally bonding the active PNIPAM hydrogel to the SU-8 patterns. It is noted that there is a large mechanical mismatch between the PNIPAM hydrogel (∼40 KPa) and SU-8 (4 GPa), which is expected to result in interfaces with large stress

concentrations. It would cause delamination during the self-morphing process. To overcome this technological barrier, a tough bonding strategy was developed by modifying previously reported ones.[35,36] In order to make a tough interface, two main requirements should be satisfied. First, the hydrogel should possess high fracture toughness that allows to dissipate large mechanical energy to the polymer matrix upon deformation. Second, the soft and stiff components should have strong adhesion. The fabrication process is schematically represented in Figure 1a and illustrated in Experimental
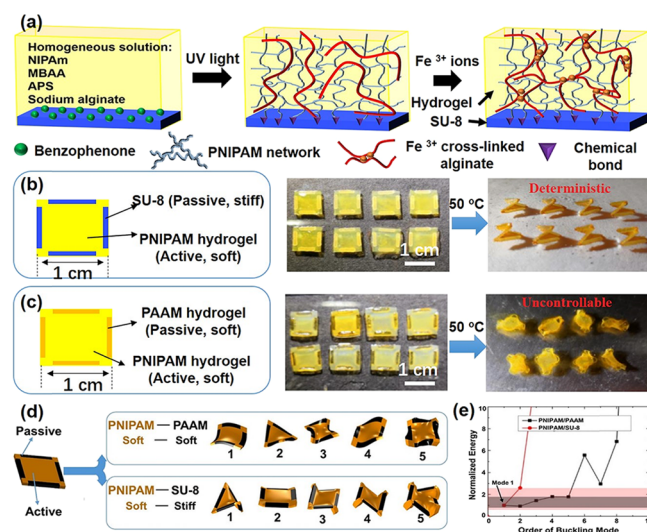

Figure 1. (a) Schematic showing formation of chemical bonding between the tough PNIPAM hydrogel and SU-8. (b) Images showing deterministic self-buckling of PNIPAM/SU-8 films. (c) Photographs showing uncontrollable self-buckling of PNIPAM/PAAM films. (d) FEA simulation results on PNIPAM/PAAM and PNIPAM/SU-8 films. (e) Elastic energy vs possible self-buckling modes for PNIPAM/PAAM and PNIPAM/SU-8 films.

Section. In brief, it includes two main steps: synthesis of a tough hydrogel and photochemical grafting of the tough hydrogel to the SU-8 patterns. The fabrication of the tough PNIPAM hydrogel followed a previous work[37] in which a reversibly ion cross-linked network of alginate was introduced to the chemically cross-linked PNIPAM via a two-step process. Compared to a normal PNIPAM hydrogel, which is fragile with a low mechanical strength of ∼5 kPa[38] and a Young's modulus of ∼10 kPa,[39] the tough PNIPAM hydrogel is highly elastic and stretchable, showing the highest tensile stress of 130 kPa and a Young's modulus of 37.2 kPa (Figure S1a). Moreover, the tough PNIPAM hydrogel well maintains the responsive property after the ionic cross-linking. After being heated above its lower critical solution temperature (LCST) of 29.3 °C (Figure S1b), its volume can still shrink to 60% of the original one (Figure S1c,d). When further increasing the temperature to 100 °C, it is dehydrated to 45% of its original volume (Figure S1e). Such a large volume shrinkage serves as the driving force to actuate the shape transformation of a PNIPAM/SU-8 film.

Fabrication of laterally bonded SU-8 patterns and PNIPAM hydrogel films is shown in Figure S2. To achieve this goal, SU-8 solution was first mixed with a 5 wt % poly-(dimethylsiloxane) (PDMS). The result shows that PDMS does not negatively affect the photopatterning property of the SU-8. After the SU-8 patterns were fabricated by photo-

lithography, they were immersed in ethanol solution with 10 wt % benzophenone for chemically grafting PNIPAM.[40] In here, the role of PDMS is to help adsorb benzophenone on the SU-8 surface.[40] It also increases the surface roughness to increase bonding sites for adhering SU-8 and the PNIPAM hydrogel (Figure S3). Finally, the precursor solution of the PNIPAM hydrogel was poured into a mold containing the SU-8 patterns followed by a photochemical grafting reaction. The qualitative results show the formation of a strong and robust interface between SU-8 and the PNIPAM tough hydrogel (Figure S4a). By contrast, SU-8 was easily peeled off if it was physically attached to the PNIPAM hydrogel (Figure S4b). These observations were further proved by a standard 90 degree peeling test (Figure S4c), which showed that the interfacial toughness was greatly increased from ∼20 to 220 J m^{-2} (Figure S4d). Due to the tough bonding between SU-8 and the hydrogel, the integrity of the SU-8/hydrogel interface can be well kept during the self-morphing process (Figure S5).

The tough SU-8/hydrogel interface facilitates out-of-plane buckling. To demonstrate the self-buckling behaviors of the hybridized films, we fabricated eight PNIPAM/SU-8 samples (Figure 1b). When heated above LCST, the PNIPAM hydrogel shrinks and imparts buckling forces to the interfaces, leading to formation of 3D structures in a controllable and deterministic manner. As shown in Figure 1b, these eight PNIPAM/SU-8 films showed all identical 3D saddle structures with dedicated and sharp edges. In a control experiment, we replaced the stiff SU-8 with a soft polyacrylamide (PAAM) hydrogel but with the same patterns. In contrast to the PNIPAM/SU-8 films, the PNIPAM/PAAM films exhibited multiple self-buckling modes and showed random 3D shapes (Figure 1c). Given that SU-8 has a much higher Young's modulus than PNIPAM, it is reasonable to hypothesize that an increased ratio of Young's modulus between the passive and active domains in the hybridized film would lower the mechanical instability, thus facilitating the self-buckling of deterministic 3D structures.

To test the hypothesis, the above self-morphing processes were simulated and analyzed by finite element analysis (FEA). In the FEA simulation, we constructed the same models as the ones showed in Figure 1b,c. SU-8 with a Young's modulus of 4 GPa and PAAM with a Young's modulus of 40 kPa act as the passive domains of the FEA models. The simulation results are shown in Figure 1d. The PNIPAM/PAAM films show five possible buckling modes. Although PNIPAM/SU-8 films also show multiple buckling modes, further elastic energy calculation of these buckling modes illustrates that only Mode 1 is possible in the experiment. The elastic energy indicates the energy needed to enable the shape transformation from an original shape to a buckled one. In other words, a higher elastic energy suggests a higher energy barrier to form such a buckling mode. Figure 1e shows the normalized elastic energy (referred to as the elastic energy in Mode 1) at different buckling modes. The PNIPAM/PAAM films show relatively low and similar energy levels for the first five possible buckling modes. It suggests that a small amount of energy input from external stimulation can easily actuate multiple buckling modes. As it is very difficult to precisely control the energy input in experiments, PNIPAM/PAAM films tend to form multiple and uncontrollable 3D shapes, agreeing well with the experimental results shown in Figure 1c. In contrast, the PNIPAM/SU-8 films show significant energy barriers from transition of Mode 1 to other modes. It indicates that the

external energy input favors to actuate Mode 1 with the lowest energy, which agrees well with the experimental result shown in Figure 1b. Herein, it is concluded that a stiff passive component in the hybridized film can effectively alleviate mechanical instability by increasing the energy barrier between shape transition modes, resulting in deterministic self-buckling.

To validate the hypothesis that existence of the SU-8 patterns can isolate local deformation of the hydrogel from neighboring morphing units, we test two distinct morphing units (S unit and T unit). When these two units were independent, they were separately morphed to a saddle surface and a tetrahedron-like structure, respectively (Figure 2a,b).
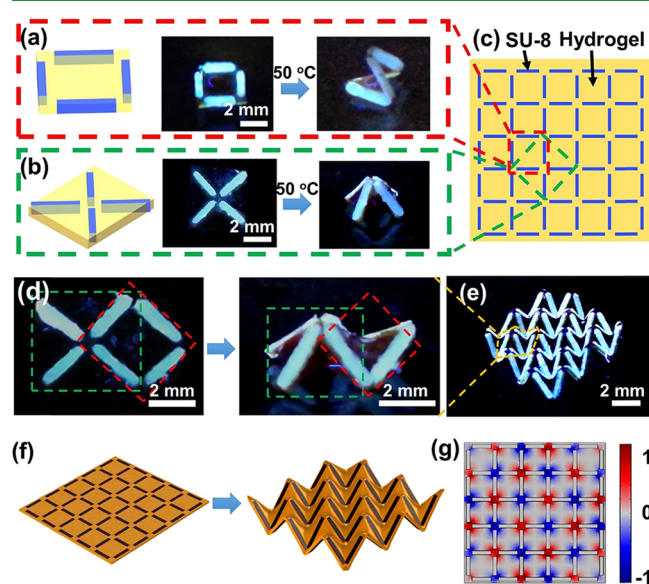

Figure 2. (a, b) Images showing self-morphing of PNIPAM/SU-8 films consisting of two different morphing units: S unit (a) and T unit (b). (c) Schematic of a PNIPAM/SU-8 film with a periodical SU-8 pattern. (d) Photograph of a 3D structure self-morphed from a PNIPAM/SU-8 film with morphing units consisting of both S unit and T unit. (e) Photograph of a self-morphed 3D peak-valley structure from a PNIPAM/SU-8 film shown in (c). (f, g) FEA modeling on the self-morphing of a PNIPAM/SU-8 film (f) and its strain distribution (g).

When these S and T units (marked red and green dash lines in Figure 2c) overlapped to form a new morphing unit, the saddle surface and tetrahedron-like structure can still form and they are well distinguishable (Figure 2d). This result is different from the ones shown in the previous literature,[23] which show that deformation of the overlapped morphing units is mutually influenced to result in distorted structures if the passive domains are too soft. In the periodical pattern (Figure 2c), the isolated unit can buckle upward or downward from a saddle structure due to the symmetric architecture in the thickness direction. These units are deformed with high cooperativity, which result in a peak-valley 3D structure, a saddle surface, and a tetrahedron-like structure (Figure 2e). It should be noted that such a 3D structure allows for complete dehydration. After the dehydration, the 3D structure became stiff, which can sustain ∼1200 times of its body weight (Figure S6). Moreover, the shape-morphing is reversible. They can recover to the planar sheets when they are immersed in water (Figure S7).

The isolated self-buckling behaviors shown in Figure 2e can be explained by FEA. As shown in Figure 2f, the FEA results

agree very well with the experimental ones. As shown in Figure 2g, in each morphing unit, the strain is only concentrated on the active hydrogel domain, and the strain in the passive SU-8 domains was close to zero. This suggested that the stiff SU-8 bars are resistant to deformation, therefore blocking the deformation from neighboring morphing units, which are well isolated. With such isolated self-morphing behaviors, it is convenient to design shape-morphing materials without concerns of mutual deformation between neighboring morphing units, which would greatly simplify the design. In addition, other SU-8 patterns were fabricated to self-morph various 3D peak-valley structures (Figure S8).

In addition to aforementioned advantages of using the SU-8 as the passive components in the hybridized polymer films, they can also add new features to the self-buckling of the hydrogel. For instance, they can fold the stiff areas continuously along their creases without deformation of the domains.[41] In previous reports, pure soft shape-morphing hydrogels were always transformed into 3D structures with rough edges.[15,24] After being integrated with the stiff SU-8 segments, the PNIPAM/SU-8 films are beneficial for creating 3D structures with sharp edges and facets. For example, rigid patterns were used to guide the self-morphing. As shown in Figure 3a, a series of nonuniform hexagonal SU-8 facets were
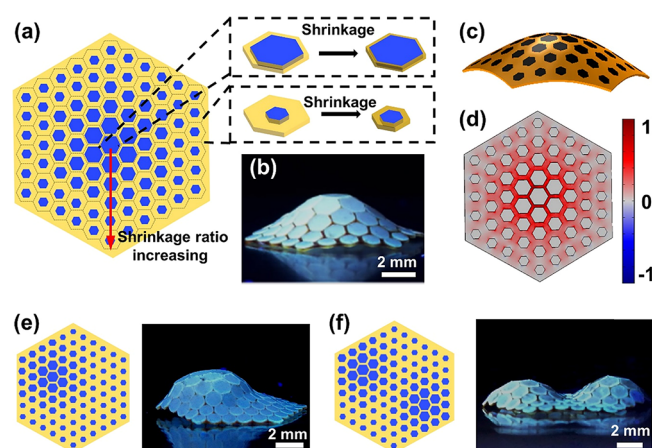

Figure 3. (a) Schematic of a PNIPAM/SU-8 film with an inhomogeneous hexagonal SU-8 pattern. (b) Photograph of a 3D structure resulting from the film shown in (a). (c, d) FEA modeling on self-morphing of a PNIPAM/SU-8 film with hexagonal SU-8 pattern (c) and its strain distribution (d). (e, f) Images of 3D structures self-morphed from PNIPAM/SU-8 films with different hexagonal SU-8 patterns.

hybridized with the PNIPAM hydrogel. The lattice spacing of these hexagonal facets was 3 mm, while the size of the stiff facets was varied (Figure 3a). Halftone gel lithography developed by Kim et al.[15] can also result in hexagonal unit cells with precisely tuned responsive property by changing the size of these hexagonal facets (Figure 3a and Figure S9). However, our approach is much simpler and more effective. The PNIPAM/SU-8 films with varied shrinkage ratios along the radial direction were obtained (Figure 3a). Upon thermal stimulation, the differential shrinkage field drove the SU-8 facets to fold, resulting in a spherical cap (Figure 3b), which was further validated by FEA (Figure 3c,d). As the volume shrinkage can be tuned in the hybridized gel film by changing the size distributions of the hexagonal SU-8 facets, different shrinkage fields were encoded in the PNIPAM/SU-8 films to

fabricate different 3D structures, such as cap-shaped surface (Figure 3e), double-peak surface (Figure 3f), four-peak surface, and turtle-like structure (Figure S10).

Besides the aforementioned hexagonal geometries, a tessellated geometry, which has been widely used in engineered structures,[42] was also adopted to fabricate various SU-8 patterns (Figure 4a,b). During the self-morphing process,
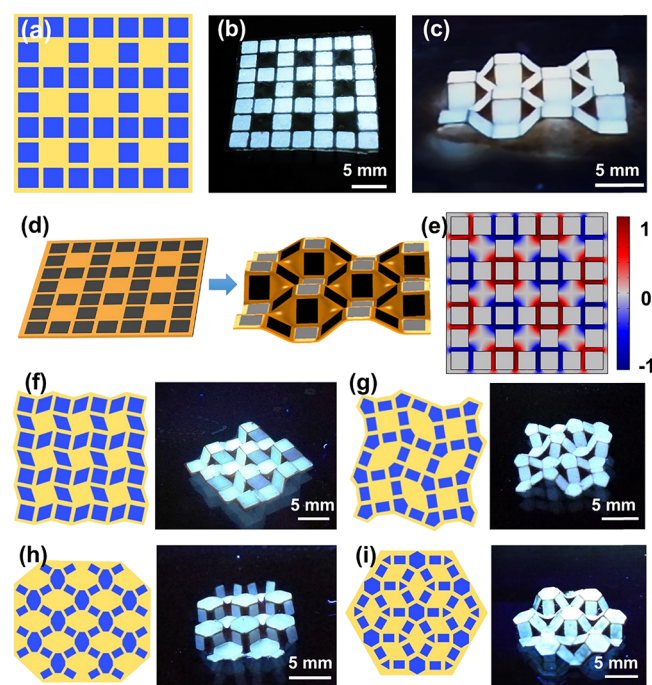

Figure 4. (a) Schematic of a PNIPAM/SU-8 film with a tessellated SU-8 pattern. (b) Photograph of a SU-8/PNIPAM hybridized film with a tessellated SU-8 pattern. (c) Photograph of a 3D structure self-morphed from the film shown in (b). (d, e) FEA modeling on the self-morphing of a PNIPAM/SU-8 film with a tessellated SU-8 pattern (d) and its strain distribution (e). (f–i) Photographs of 3D structures self-morphed from PNIPAM/SU-8 films with different SU-8 patterns.

the shrinkage of hydrogel drove them to form 3D checkerboard structures. Their shape transformation behaviors were modeled and validated by FEA (Figure 4d,e), showing good agreement with the experimental results. In addition, we also designed various SU-8 patterns, as shown in Figure 4f–i. Depending on the geometry and location of these stiff SU-8 facets, different types of 3D tessellation structures were obtained.

Finally, we explored the application of the self-buckled 3D structures as the acoustic metamaterials. Possible acoustic metamaterials were first conceived (Figure 5a and Figure S11). The most representative one shown in Figure 5a consists of a series of diagonally distributed wedge bulges. The resonant scattering of such a periodic structure may show phononic band gaps for acoustic energy blocking. To validate this hypothesis, the FEA simulation was applied to calculate normalized acoustic frequency response (AFR), which is represented by the square of a ratio of the transmitted sound power (P_{tr}) and incident sound power (P_{in}) at different frequencies. The simulation was performed by a dynamically coupled piezoelectric-circuit-structural-acoustic module integrated in COMSOL Multiphysics. In the simulation, frequency of the input signal varying from 0 to 10,000 Hz was applied
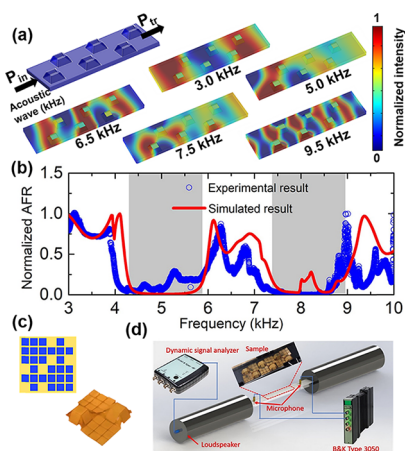
Figure 5. (a) FEA model of an acoustic material and its acoustic pressure field distributions at frequencies of 3.0, 5.0, 6.5, 7.5, and 9.5 kHz. (b) Normalized simulation AFR of the acoustic material shown in (a) and normalized experimental AFR from the 3D structure shown in (c). (c) Photograph of a 3D structure self-morphed from a corresponding PNIPAM/SU-8 film. (d) Schematic of an acoustic testing apparatus.

and then P_{tr} was collected. Figure 5a shows the acoustic pressure field distribution when the input sounds with frequencies of 3.0, 5.0, 6.5, 7.5, and 9.5 kHz were applied. It shows that this 3D structure can effectively block the energy of the input sounds at a frequency range of 5.0 and 7.5 kHz. Figure 5b shows a simulated transmission spectrum of this 3D structure at the input frequencies varying from 3 to 10 kHz. It shows two profound transmission losses in the frequency ranges of ~4000−~6000 Hz and ~7000−9000 Hz, indicating formation of two phononic band gaps in this 3D structure.

To validate these simulation results, we fabricated a hybridized gel film that was later self-buckled to a 3D structure that showed the same shape, as shown in Figure 5a. Upon thermal stimulation, the hybridized film was transformed into the desired 3D structure with diagonally distributed wedge bulges (Figure 5c). They were then loaded into an acoustic testing apparatus and subjected to the testing procedure, as shown in our past works[43,44] (Figure 5d). The normalized AFR from the testing is plotted in Figure 5b. The experimental AFR well overlapped with the simulation AFR. The two peaks ranging from 4 to 6 kHz and 7 to 9 kHz were clearly observed, showing profound phononic band gaps from this 3D acoustic metamaterial. We believe that this performance can be partially attributed to the self-morphed 3D structure with sharp edges and facets. This successful demonstration would pave a new route to fabricating acoustic metamaterials, which allows for on-demand deployment of 3D structures that can be self-assembled from the planar films.

CONCLUSIONS

In summary, we developed a soft-stiff hybridized self-morphing material for fabricating responsive 3D structures with deterministic 3D-shaping behaviors. The deployed SU-8 patterns in the hybridized film increased the energy barrier among shape-buckling transition modes and isolated the local deformation from the negative impact of the neighboring morphing units in the responsive PNIPAM hydrogel, therefore effectively alleviating the uncontrollability and uncertainty in the self-buckling process. Upon thermal stimulation, the

PNIPAM/SU-8 hybridized films exhibited deterministic and complex 3D shape transformation from their planar counterparts. As one of the promising applications, the hybridized films can be tailored for effective noise mitigation and cancellation. The present study would provide a new route to fabricating smart and multifunctional materials for widespread applications in metamaterials, soft robotics, and 3D electronics.

EXPERIMENTAL SECTION

Fabrication of PNIPAM Hydrogel. *N*-isopropylacrylamide (NIPAM) monomer (300 mg), Na-alginate powder (43 mg), methylene-*N*,*N*′-bis(acrylamide) (MBAA) cross-linker (0.3 mg), and polymerization accelerator *N*,*N*,*N*′,*N*′-tetramethylethylenediamine (TEMED) (10 μL) were dissolved in 2 g of deionized water. Then, 0.5 mL of 1% ammonium peroxodisulfate (APS) aqueous initiator solution was added and mixed thoroughly. The resulting solution was transferred into a mold. After curing for 30 min in an ice bath, the solution was gelatinized to produce the Na-alginate/PNIPAM hydrogel. Then, the strips were immersed in a 1 mol/L $Fe(NO_3)_3$ aqueous solution for 1 h. During this process, the Fe^{3+} ions diffused into the hydrogel matrix and replaced the Na^+ ions to cross-link the alginate polymer to form a tough Fe-alginate/PNIPAM hydrogel.

Fabrication of SU-8 Patterns. Clean glass slides were coated with a thin poly(vinyl alcohol) (PVA) layer, which served as a sacrifice layer. Before coating the SU-8 resist on the glass slides, the SU-8 resist was first mixed with 5 wt % PDMS. In details, 0.25 g of part A and 0.25 of part B of silicone rubber Ecoflex 00-30 (Smooth-On, PA, USA) were added to 9.5 g of SU-8 solution (SU-82000 series from MicroChem) and mixed thoroughly. SU-8 sheets with 300 μm thickness were obtained by dropping the SU-8 resist (250 mg) on the glass slides (2.5 cm × 2.5 cm). SU-8 (300 μm) was chosen, which enabled to resist the deformation caused by shrinkage of the PNIPAM hydrogel. As a control, a thin SU-8 film (such as 45 μm) cannot resist the deformation, resulting in uncontrollable shape transformation (Figure S12). Then, a scraper was used to spread the SU-8 solution at 80 °C. The SU-8 solution was spread to cover every edge of the glass substrate, which could prevent the solution from shrinking during the baking process due to surface tension. The SU-8 solution was baked on a hotplate at 120 °C for 2 h. After baking, the slides were cooled down, kept at 60 °C for 5 min, and then slowly cooled to room temperature. To prepare SU-8 patterns, the SU-8 sheets were exposed to UV light through a homemade photomask with the designed patterns for 30 s using an UVP B-100 series UV lamp (21.7 mW/cm²). The postexposure baking was carried out at 90 °C for 10 min. After slowly cooling to room temperature, the SU-8 patterns were developed in an SU-8 developer and then baked at 90 °C for 5 min to remove the residual organic solvent. After that, a second UV exposure (5 min) was used to further cross-link the SU-8.

Fabrication of PNIPAM/SU-8 Hydrogel Composite. The obtained SU-8 patterns were first treated with benzophenone by immersing them in benzophenone solution (10 wt % in ethanol) for 5 min at room temperature. Then, the SU-8 patterns were washed with methanol and dried with nitrogen gas. After that, the hydrogel precursor solution containing NIPAM, Na-alginate powder, APS, TEMED, and MBAA was filled in between the SU-8 patterns. A doctor blade was used to remove the excessive solution that was on top of the SU-8 patterns. Then, the surface was covered by another glass slide. It should be noted that the synthetic hydrogel was very sticky to the glass slide, making it difficult to remove the top glass slide. Therefore, we coated a thin layer of poly(vinylidene difluoride) (PVDF) (20% PVDF in DMF solution) at 1000 rpm for 30 s on the glass slide. Then, the sample was exposed to UV radiation in an ice bath for 30 min. After the reaction, the top glass slide can be easily removed, leaving the PVDF thin sheet covered on the SU-8/hydrogel hybridized film. After that, one drop of acetone was added on the surface of PVDF. The PVDF would be swollen by acetone and easily peeled off from the SU-8/hydrogel film by a tweezer. The resulting

SU-8/hydrogel film was then immersed in 1 mol/L Fe(NO₃)₃ aqueous solution for 1 h to obtain an Fe-alginate/PNIPAM hydrogel pattern that as laterally stitched to the SU-8 pattern. The free-standing film was peeled off from the substrate by a doctor blade. Finally, the edges of the SU-8/hydrogel hybridized film were trimmed by a knife.

Fabrication of PNIPAM/PAAM Hydrogel Composite. The PNIPAM/PAAM film was fabricated by a two-step polymerization process. A precursor solution of PAAM was poured into a reaction cell composed of two glass substrates separated by a 300 μm-thick polyimide spacer. The precursor solution was prepared by adding the AAM monomer (300 mg), Na-alginate powder (43 mg), MBAA cross-linker (0.3 mg), and polymerization accelerator TEMED (10 μL) in 2 g of deionized water. After the hydrogel was cured at room temperature, the films were cut by a CO_2 laser to obtain PAAM patterns. Then, a PNIPAM hydrogel precursor solution containing NIPAM, Na-alginate powder, APS, TEMED, and MBAA was filled in between the PAAM patterns. A doctor blade was used to remove the excessive solution that was on top of the SU-8 patterns. Then, the surface was covered by another PVDF coated glass slide. After the reaction, the top glass slide was easily removed, leaving the PVDF thin sheet covered on the PNIPAM/PAAM film. After that, one drop of acetone was added on the surface of PVDF. The PVDF would be swollen by acetone and then easily peeled off from the PNIPAM/PAAM film by a tweezer. The resulting hybridized hydrogel film was then immersed in 1 mol/L Fe(NO₃)₃ aqueous solution for 1 h and then was peeled off from the substrate by a blade. Finally, the edges were trimmed by a knife.

Measurements. Shrinkage ratios of the PNIPAM hydrogel were calculated by measuring dimension changes of samples in as-prepared states and dried states. In detail, it is expressed as the ratio of changed length ΔL to the original length L of an investigated sample. The LCST of the PNIPAM hydrogel was measured by a differential scanning calorimeter (DSC) (PerkinElmer DSC8500). Tensile and peeling tests were conducted on a Mark-10 ESM303 tensile tester. Images of SU-8/PNIPAM hydrogel composite sheets were taken by an optical microscope (MU130, AmScope). The videos and photographs of self-morphing behaviors of SU-8/PNIPAM films were taken by a smart phone under UV light. Acoustic frequency response of the acoustic metamaterial was tested in a chamber consisting of two cylinder tubes with an inner diameter of 50 mm and one rectangular tube with an inner width of 20 mm, length of 200 mm, and height of 2 mm. The cylinder and rectangular tubes were made from aluminum and acrylic, respectively. To test its acoustic properties, we fabricated an array of three unit cells. In the test, it was placed in the middle of a tube with a rectangular cross section. A loudspeaker was mounted in one end of the tube, while the other end was open. The microphone (PCB model: 378C01) was placed on the surface of the rectangular tube. The signals were generated by a B&K dynamic signal analyzer and captured by B&K type 3050 DAQ. The signals generated here were white noise. All the possible acoustic leaking points were sealed by plasticine before testing.

FEA Simulation. The finite element analysis (FEA) simulations were performed by COMSOL Multiphysics. To decrease the computational cost and simplify the data analysis, both the PNIPAM hydrogel and SU-8 were assumed to be the linearly elastic isotropic materials. Physical properties of PNIPAM hydrogels were set: Young's modulus of 40 kPa, Poisson's ratio of 0.4, thermal expansion coefficient of -10×10^{-6}/K, and density of 900 kg/m³. Physical properties of PAAM hydrogels were set: Young's modulus of 40 kPa, Poisson's ratio of 0.4, thermal expansion coefficient of 0/K, and density of 900 kg/m³. Physical properties of SU-8 were set: Young's modulus of 4 GPa, Poisson's ratio of 0.22, thermal expansion coefficient of 0/K, and density of 1190 kg/m³. FEA models were designed the same way as the experimental ones. During the simulation, the boundary was totally free, and then the thermal expansion field was applied in both the PNIPAM hydrogel and SU-8. When thermal energy was applied, the hybridized film showed shape deformation to store the elastic energy. Such energy was calculated through a stationary and linear buckling study. From the calculation, different types of buckling modes were obtained.[45,46] The stored elastic energy in different buckling modes was also calculated. Instead of tracking the transient process, we focused on the total elastic energies of deformation modes under equilibrium conditions.

■ ASSOCIATED CONTENT

Ⓢ Supporting Information

The Supporting Information is available free of charge at https://pubs.acs.org/doi/10.1021/acsami.0c01115.

Tensile test, DSC curve of the tough PNIPAM hydrogel, schematic of fabrication processes of the PNIPAM/SU-8 hydrogel composite, optical images of surface morphologies of pure SU-8 and SU-8/PDMS mixture, details of peeling tests, photographs showing shrinkage of PNIPAM/SU-8 hexagonal unit cells, and additional optical images of assembled 3D structures (PDF)

■ AUTHOR INFORMATION

Corresponding Authors

Guoliang Huang − *Department of Mechanical and Aerospace Engineering, University of Missouri, Columbia, Missouri 65211, United States*; Email: huangg@missouri.edu

Jian Lin − *Department of Mechanical and Aerospace Engineering, Department of Electrical Engineering and Computer Science, and Department of Physics and Astronomy, University of Missouri, Columbia, Missouri 65211, United States*; ⓘ orcid.org/0000-0002-4675-2529; Email: linjian@missouri.edu

Authors

Heng Deng − *Department of Mechanical and Aerospace Engineering, University of Missouri, Columbia, Missouri 65211, United States*

Xianchen Xu − *Department of Mechanical and Aerospace Engineering, University of Missouri, Columbia, Missouri 65211, United States*

Cheng Zhang − *Department of Mechanical and Aerospace Engineering, University of Missouri, Columbia, Missouri 65211, United States*

Jheng-Wun Su − *Department of Mechanical and Aerospace Engineering, University of Missouri, Columbia, Missouri 65211, United States*

Complete contact information is available at:
https://pubs.acs.org/10.1021/acsami.0c01115

Author Contributions

‖H.D. and X.X. contributed equally to this work.

Notes

The authors declare no competing financial interest.

■ ACKNOWLEDGMENTS

■ REFERENCES

(1) Mayer, G. Rigid Biological Systems as Models for Synthetic Composites. *Science* **2005**, *310*, 1144−1147.

(2) Vatankhah-Varnosfaderani, M.; Keith, A. N.; Cong, Y.; Liang, H.; Rosenthal, M.; Sztucki, M.; Clair, C.; Magonov, S.; Ivanov, D. A.; Dobrynin, A. V.; Sheiko, S. S. Chameleon-Like Elastomers with Molecularly Encoded Strain-Adaptive Stiffening and Coloration. *Science* **2018**, *359*, 1509−1513.

(3) Teyssier, J.; Saenko, S. V.; van der Marel, D.; Milinkovitch, M. C. Photonic Crystals Cause Active Colour Change in Chameleons. *Nat. Commun.* **2015**, *6*, 6368.

(4) Gu, G. X.; Takaffoli, M.; Buehler, M. J. Hierarchically Enhanced Impact Resistance of Bioinspired Composites. *Adv. Mater.* **2017**, *29*, 1700060.

(5) Gu, G. X.; Chen, C.-T.; Richmond, D. J.; Buehler, M. J. Bioinspired Hierarchical Composite Design Using Machine Learning: Simulation, Additive Manufacturing, and Experiment. *Mater. Horiz.* **2018**, *5*, 939−945.

(6) Yang, Z.; Gao, F.; Shi, X.; Lin, X.; Gao, Z.; Chong, Y.; Zhang, B. Topological Acoustics. *Phys. Rev. Lett.* **2015**, *114*, 114301.

(7) Wang, J.; Mei, J. Topological Valley-Chiral Edge States of Lamb Waves in Elastic Thin Plates. *Appl. Phys. Express* **2018**, *11*, No. 057302.

(8) Li, S.; Zhao, D.; Niu, H.; Zhu, X.; Zang, J. Observation of Elastic Topological States in Soft Materials. *Nat. Commun.* **2018**, *9*, 1370.

(9) Oyefusi, A.; Chen, J. Reprogrammable Chemical 3D Shaping for Origami, Kirigami, and Reconfigurable Molding. *Angew. Chem., Int. Ed.* **2017**, *56*, 8250−8253.

(10) Eckel, Z. C.; Zhou, C.; Martin, J. H.; Jacobsen, A. J.; Carter, W. B.; Schaedler, T. A. Additive Manufacturing of Polymer-Derived Ceramics. *Science* **2016**, *351*, 58−62.

(11) Zhang, Y.; Zhang, F.; Yan, Z.; Ma, Q.; Li, X.; Huang, Y.; Rogers, J. A. Printing, Folding and Assembly Methods for Forming 3D Mesostructures in Advanced Materials. *Nat. Rev. Mater.* **2017**, *2*, 17019.

(12) Zhang, C.; Su, J.-W.; Deng, H.; Xie, Y.; Yan, Z.; Lin, J. Reversible Self-Assembly of 3D Architectures Actuated by Responsive Polymers. *ACS Appl. Mater. Interfaces* **2017**, *9*, 41505−41511.

(13) Zhang, C.; Deng, H.; Xie, Y.; Zhang, C.; Su, J. W.; Lin, J. Stimulus Responsive 3D Assembly for Spatially Resolved Bifunctional Sensors. *Small* **2019**, *15*, 1904224.

(14) Liu, Y.; Genzer, J.; Dickey, M. D. "2D or not 2D": Shape-Programming Polymer Sheets. *Prog. Polym. Sci.* **2016**, *52*, 79−106.

(15) Kim, J.; Hanna, J. A.; Byun, M.; Santangelo, C. D.; Hayward, R. C. Designing Responsive Buckled Surfaces by Halftone Gel Lithography. *Science* **2012**, *335*, 1201−1205.

(16) Jamal, M.; Zarafshar, A. M.; Gracias, D. H. Differentially Photo-Crosslinked Polymers Enable Self-Assembling Microfluidics. *Nat. Commun.* **2011**, *2*, 527.

(17) Yu, X.; Zhou, J.; Liang, H.; Jiang, Z.; Wu, L. Mechanical Metamaterials Associated with Stiffness, Rigidity and Compressibility: A Brief Review. *Prog. Mater. Sci.* **2018**, *94*, 114−173.

(18) Deng, H.; Zhang, C.; Su, J.-W.; Xie, Y.; Zhang, C.; Lin, J. Bioinspired Multi-Responsive Soft Actuators Controlled by Laser Tailored Graphene Structures. *J. Mater. Chem. B* **2018**, *6*, 5415−5423.

(19) Hubbard, A. M.; Cui, W.; Huang, Y.; Takahashi, R.; Dickey, M. D.; Genzer, J.; King, D. R.; Gong, J. P. Hydrogel/Elastomer Laminates Bonded via Fabric Interphases for Stimuli-Responsive Actuators. *Matter* **2019**, *1*, 674−689.

(20) Deng, H.; Dong, Y.; Zhang, C.; Xie, Y.; Zhang, C.; Lin, J. An Instant Responsive Polymer Driven by Anisotropy of Crystal Phases. *Mater. Horiz.* **2018**, *5*, 99−107.

(21) Deng, H.; Dong, Y.; Su, J.-W.; Zhang, C.; Xie, Y.; Zhang, C.; Maschmann, M. R.; Lin, Y.; Lin, J. Bioinspired Programmable Polymer Gel Controlled by Swellable Guest Medium. *ACS Appl. Mater. Interfaces* **2017**, *9*, 30900−30908.

(22) Kempaiah, R.; Nie, Z. From Nature to Synthetic Systems: Shape Transformation in Soft Materials. *J. Mater. Chem. B* **2014**, *2*, 2357−2368.

(23) Wang, Z. J.; Zhu, C. N.; Hong, W.; Wu, Z. L.; Zheng, Q. Cooperative Deformations of Periodically Patterned Hydrogels. *Sci. Adv.* **2017**, *3*, No. e1700348.

(24) Klein, Y.; Efrati, E.; Sharon, E. Shaping of Elastic Sheets by Prescription of non-Euclidean Metrics. *Science* **2007**, *315*, 1116−1120.

(25) Nojoomi, A.; Arslan, H.; Lee, K.; Yum, K. Bioinspired 3D Structures with Programmable Morphologies and Motions. *Nat. Commun.* **2018**, *9*, 3705.

(26) Grimm, D.; Bof Bufon, C. C.; Deneke, C.; Atkinson, P.; Thurmer, D. J.; Schäffel, F.; Gorantla, S.; Bachmatiuk, A.; Schmidt, O. G. Rolled-up Nanomembranes as Compact 3D Architectures for Field Effect Transistors and Fluidic Sensing Applications. *Nano Lett.* **2013**, *13*, 213−218.

(27) Xu, S.; Yan, Z.; Jang, K. I.; Huang, W.; Fu, H.; Kim, J.; Wei, Z.; Flavin, M.; McCracken, J.; Wang, R.; Badea, A.; Liu, Y.; Xiao, D.; Zhou, G.; Lee, J.; Chung, H. U.; Cheng, H.; Ren, W.; Banks, A.; Li, X.; Paik, U.; Nuzzo, R. G.; Huang, Y.; Zhang, Y.; Rogers, J. A. Assembly of Micro/nanomaterials into Complex, Three-dimensional Architectures by Compressive Buckling. *Science* **2015**, *347*, 154−159.

(28) Zhang, Y.; Yan, Z.; Nan, K.; Xiao, D.; Liu, Y.; Luan, H.; Fu, H.; Wang, X.; Yang, Q.; Wang, J.; Ren, W.; Si, H.; Liu, F.; Yang, L.; Li, H.; Wang, J.; Guo, X.; Luo, H.; Wang, L.; Huang, Y.; Rogers, J. A. A Mechanically Driven form of Kirigami as a Route to 3D Mesostructures in Micro/nanomembranes. *Proc. Natl. Acad. Sci.* **2015**, *112*, 11757−11764.

(29) Yan, Z.; Zhang, F.; Liu, F.; Han, M.; Ou, D.; Liu, Y.; Lin, Q.; Guo, X.; Fu, H.; Xie, Z.; Gao, M.; Huang, Y.; Kim, J.; Qiu, Y.; Nan, K.; Kim, J.; Gutruf, P.; Luo, H.; Zhao, A.; Hwang, K.-C.; Huang, Y.; Zhang, Y.; Rogers, J. A. Mechanical Assembly of Complex, 3D Mesostructures from Releasable Multilayers of Advanced Materials. *Sci. Adv.* **2016**, *2*, No. e1601014.

(30) Ma, M.; Guo, L.; Anderson, D. G.; Langer, R. Bio-Inspired Polymer Composite Actuator and Generator Driven by Water Gradients. *Science* **2013**, *339*, 186−189.

(31) Zhang, Y. S.; Khademhosseini, A. Advances in Engineering Hydrogels. *Science* **2017**, *356*, eaaf3627.

(32) Ionov, L. Biomimetic Hydrogel-Based Actuating Systems. *Adv. Funct. Mater.* **2013**, *23*, 4555−4570.

(33) Le, X.; Lu, W.; Zhang, J.; Chen, T. Recent Progress in Biomimetic Anisotropic Hydrogel Actuators. *Adv. Sci.* **2019**, *6*, 1801584.

(34) Wang, Z. J.; Hong, W.; Wu, Z. L.; Zheng, Q. Site-Specific Pre-Swelling-Directed Morphing Structures of Patterned Hydrogels. *Angew. Chem., Int. Ed.* **2017**, *56*, 15974−15978.

(35) Lin, S.; Yuk, H.; Zhang, T.; Parada, G. A.; Koo, H.; Yu, C.; Zhao, X. Stretchable Hydrogel Electronics and Devices. *Adv. Mater.* **2016**, *28*, 4497−4505.

(36) Yuk, H.; Zhang, T.; Lin, S.; Parada, G. A.; Zhao, X. Tough Bonding of Hydrogels to Diverse non-Porous Surfaces. *Nat. Mater.* **2016**, *15*, 190−196.

(37) Zheng, W. J.; An, N.; Yang, J. H.; Zhou, J.; Chen, Y. M. Tough Al-Alginate/poly(N-isopropylacrylamide) Hydrogel with Tunable LCST for Soft Robotics. *ACS Appl. Mater. Interfaces* **2015**, *7*, 1758−1764.

(38) Haraguchi, K.; Takehisa, T.; Fan, S. Effects of Clay Content on the Properties of Nanocomposite Hydrogels Composed of Poly (N-isopropylacrylamide) and Clay. *Macromolecules* **2002**, *35*, 10162−10171.

(39) Zhang, X.-Z.; Wu, D.-Q.; Chu, C.-C. Synthesis, Character-ization and Controlled Drug Release of Thermosensitive IPN−PNIPAAm Hydrogels. *Biomaterials* **2004**, *25*, 3793−3805.

(40) Yuk, H.; Zhang, T.; Parada, G. A.; Liu, X.; Zhao, X. Skin-Inspired Hydrogel−Elastomer Hybrids with Robust Interfaces and Functional Microstructures. *Nat. Commun.* **2016**, *7*, 12028.

(41) Tachi, T. Rigid-Foldable Thick Origami. *Origami 5* **2011**, *5*, 253−264.

(42) Fathers, R. K.; Gattas, J. M.; You, Z. Quasi-Static Crushing of Eggbox, Cube, and Modified Cube Foldcore Sandwich Structures. *Int. J. Mech. Sci.* **2015**, *101*, 421−428.

(43) Chen, H.; Li, X. P.; Chen, Y. Y.; Huang, G. L. Wave Propagation and Absorption of Sandwich Beams Containing Interior Dissipative Multi-Resonators. *Ultrasonics* **2017**, *76*, 99−108.

(44) Li, J.; Zhou, X.; Huang, G.; Hu, G. Acoustic Metamaterials Capable of Both Sound Insulation and Energy Harvesting. *Smart Mater. Struct.* **2016**, *25*, No. 045013.

(45) Xue, R.; Li, R.; Du, Z.; Zhang, W.; Zhu, Y.; Sun, Z.; Guo, X. Kirigami Pattern Design of Mechanically Driven Formation of Complex 3D Structures Through Topology Optimization. *Extreme Mech. Lett.* **2017**, *15*, 139−144.

(46) An, N.; Li, M.; Zhou, J. Predicting Origami-Inspired Programmable Self-Folding of Hydrogel Trilayers. *Smart Mater. Struct.* **2016**, *25*, 11LT02.